

Quasi-phase-matched supercontinuum-generation in photonic waveguides

Daniel D. Hickstein,^{1,*} Grace C. Kerber,^{1,2} David R. Carlson,¹ Lin Chang,³ Daron Westly,⁴ Kartik Srinivasan,⁴ Abijith Kowligy,¹ John E. Bowers,³ Scott A. Diddams,^{1,5} and Scott B. Papp^{1,5}

¹*Time and Frequency Division, National Institute of Standards and Technology, Boulder, Colorado 80305, U.S.A.*

²*Gustavus Adolphus College, Saint Peter, Minnesota 56082, U.S.A.*

³*Department of Electrical and Computer Engineering, University of California, Santa Barbara, California 93106, U.S.A.*

⁴*Center for Nanoscale Science and Technology, NIST, Gaithersburg, Maryland 20899, U.S.A.*

⁵*Department of Physics, University of Colorado, Boulder, Colorado, 80309, U.S.A.*

(Dated: October 28, 2021)

Supercontinuum generation in integrated photonic waveguides is a versatile source of broadband light, and the generated spectrum is largely determined by the phase-matching conditions. Here we show that quasi-phase-matching via periodic modulations of the waveguide structure provides a useful mechanism to control the evolution of ultrafast pulses during supercontinuum generation. We experimentally demonstrate quasi-phase-matched supercontinuum to the TE₂₀ and TE₀₀ waveguide modes, which enhances the intensity of the SCG in specific spectral regions by as much as 20 dB. We utilize higher-order quasi-phase-matching (up to the 16th order) to enhance the intensity in numerous locations across the spectrum. Quasi-phase-matching adds a unique dimension to the design-space for SCG waveguides, allowing the spectrum to be engineered for specific applications.

Supercontinuum generation (SCG) is a $\chi^{(3)}$ nonlinear process where laser pulses of relatively narrow bandwidth can be converted into a continuum with large spectral span [1–3]. SCG has numerous applications, including self-referencing frequency combs [4–6], microscopy [7], spectroscopy [8], and tomography [9]. SCG is traditionally accomplished using bulk crystals or nonlinear fiber, but recently, “photonic waveguides” (on-chip waveguides produced using nanofabrication techniques) have proven themselves as a versatile platform for SCG, offering small size, high nonlinearity, and increased control over the generated spectrum [10–19]. The spectral shape and efficiency of SCG is determined by the input pulse parameters, the nonlinearity of the material, and the refractive index of the waveguide, which determines the phase-matching conditions.

Specifically, when phase-matching between a soliton and quasi-continuous-wave (CW) light is achieved, strong enhancements of the intensity of the supercontinuum spectrum can occur in certain spectral regions. These spectral peaks are often referred to as a dispersive waves (DWs) [2, 20–22], and they are often crucial for providing sufficient spectral brightness for many applications. The soliton-DW phase-matching condition is typically satisfied by selecting a material with a favorable refractive index profile and engineering the dimensions of the waveguide to provide DWs at the desired wavelengths [15, 16]. However, there are limitations to the refractive index profile that can be achieved by adjusting only the waveguide cross-section. Quasi-phase-matching (QPM) takes a different approach, utilizing periodic modulations of the material nonlinearity to achieve an end-result similar to true phase-matching [23–26]. QPM is routinely employed to achieve high conversion efficiency for nonlinear

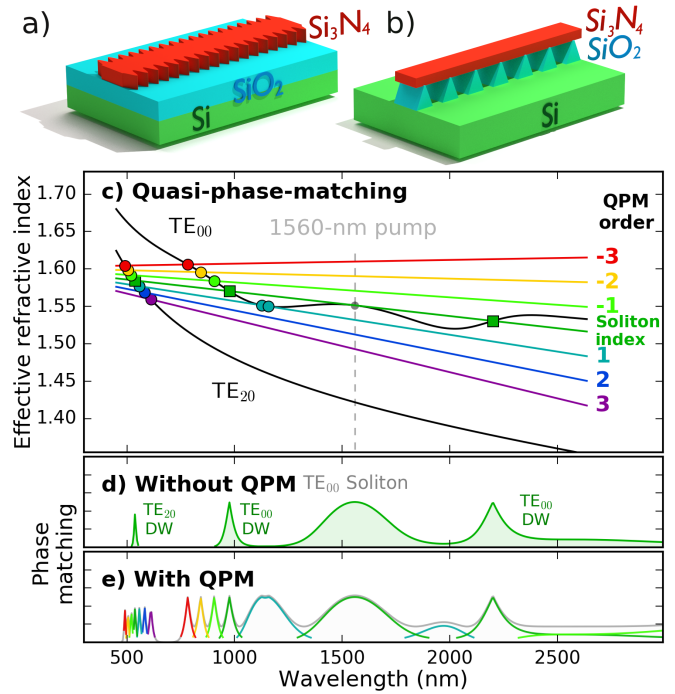


FIG. 1. a,b) Quasi-phase-matching (QPM) of supercontinuum generation in on-chip photonic waveguides can be achieved via waveguide-width modulation (a) or cladding-modulation (b). c) When the effective index of the soliton in the TE₀₀ mode (“soliton index”) intersects the effective index of a waveguide mode (black curves), phase matching to dispersive waves (DWs) is achieved (green squares) and a spectrum with several peaks (d) is generated. The periodic modulation of the waveguide can enable numerous QPM orders, both positive and negative, which can allow QPM-DW generation to the fundamental mode and to higher-order modes (circles), producing a spectrum with many peaks (e). Note: the index curvature is exaggerated to better show phase-matching.

* danhickstein@gmail.com

processes such as second harmonic generation and different frequency generation, and QPM can also be used to satisfy the phase-matching conditions for DW generation [27–31].

Here we show that periodic modulations of the effective mode area can enable QPM of DW generation in photonic silicon nitride (Si_3N_4) waveguides, enhancing the intensity of the supercontinuum in specific spectral regions determined by the modulation period. Experimentally, we utilize a sinusoidal modulation of the waveguide width to enable first-order QPM to the TE_{20} mode. Additionally, we demonstrate that periodic SiO_2 under-cladding provides numerous orders of QPM to both the TE_{20} and TE_{00} modes. This quasi-phase-matched dispersive-wave (QPM-DW) scheme provides a fundamentally different approach to phase-matching in SCG, allowing light to be generated outside the normal wavelength range, and providing separate control over the group-velocity dispersion (GVD) of the waveguide (which influences soliton propagation) and DW phase-matching, capabilities that are desirable for many applications of SCG.

In the regime of anomalous GVD, the nonlinearity of the material can balance GVD and allow pulses to propagate while remaining temporally short. Such solitons can propagate indefinitely, unless perturbed [2, 3]. However, in the presence of higher-order dispersion, some wavelengths of quasi-CW light may propagate at the same phase velocity as the soliton. Light at these wavelengths can “leak out” of the soliton, in the form of DW radiation [2], which is also referred to as “resonant radiation” [20, 21] or “optical Cherenkov radiation” [22]. In the SCG process, higher-order solitons undergo soliton fission and can convert significant amounts of energy into DW radiation [2]. The phase-matching condition for DW generation (in the absence of QPM) is simply [22]

$$n(\lambda_s) + (\lambda - \lambda_s) \frac{dn}{d\lambda}(\lambda_s) + \gamma p \lambda = n(\lambda), \quad (1)$$

where λ is wavelength, λ_s is the center wavelength of the soliton, n is the effective index of the waveguide, $\frac{dn}{d\lambda}(\lambda_s)$ is the slope of the n -versus- λ curve evaluated at λ_s , γ is the effective nonlinearity of the waveguide, and p is the peak power. The left side of Eq. 1 represents the effective index of the soliton while the right side represents the effective index of the DW. This equation has a simple graphical interpretation; because all wavelengths in the soliton travel with the same group velocity, the effective index of the soliton is simply a straight line (Fig. 1c). Where this line crosses the refractive index curve for any waveguide mode (black lines in Fig. 1c), DW generation is phase matched.

Periodic modulations of the waveguide change the effective area of the mode, modulating both γ and the GVD, enabling QPM-DW generation (see Supplemental Materials, section IV). The contribution of a modulation (with period Λ) to the wavevector phase-mismatch will be $k_{\text{QPM}} = 2\pi q/\Lambda$, where q is the QPM order and can be any positive or negative integer. Thus, the phase-

matching condition for dispersive wave generation, in the presence of QPM is

$$\underbrace{n(\lambda_s) + (\lambda - \lambda_s) \frac{dn}{d\lambda}(\lambda_s) + \gamma p \lambda}_{\text{Soliton index}} = \underbrace{n(\lambda)}_{\text{DW index}} + \underbrace{\frac{2\pi q \lambda}{\Lambda}}_{\text{QPM}}. \quad (2)$$

This phase-matching condition has a similar graphical interpretation; an additional line is drawn for each QPM order, with curve-crossings indicating QPM of DWs (Fig. 1c).

In addition to satisfying the QPM condition (Eq. 2), three additional requirements must be met for efficient DW generation. (1) The QPM order q must be a strong Fourier component of the periodic modulation. (2) There must be overlap between the spatial mode of the soliton and the mode of the DW. (3) The DW must be located in a spectral region where the soliton has significant intensity, a requirement that applies regardless of the phase-matching method.

Experimentally, we explore two different approaches for QPM-DW generation in Si_3N_4 waveguides: width-modulated waveguides and cladding-modulated waveguides. The width-modulated Si_3N_4 waveguides (Fig. 1a) are fully SiO_2 -clad and have a thickness of 750 nm, a maximum width of 1500 nm, and an overall length of 15 mm. Over a 6-mm central region, the width is modulated sinusoidally from 1250 to 1500 nm. Multiple waveguides are fabricated on the same silicon chip, and each waveguide has a different width modulation period, which ranges from 5.5 to 6.5 μm . Each cladding-modulated waveguide (Fig. 1b) consists of a 700-nm-thick Si_3N_4 waveguide that is completely air-clad, except for underlying SiO_2 support structures. The support structures are placed every 200 μm along the waveguide, and each one contacts the Si_3N_4 waveguide for approximately 20 μm . For the cladding-modulated waveguides, the modulation period is kept constant, but several waveguide widths are tested, ranging from 3000 to 4000 nm.

We generate supercontinuum by coupling ~ 80 fs pulses of 1560-nm light from a compact 100 MHz Er-fiber frequency comb [32]. The power is adjusted using a computer-controlled rotation-mount containing a half-waveplate, which is placed before a polarizer. The polarization is set to horizontal (i.e., parallel to the Si-wafer surface and along the long dimension of the rectangular Si_3N_4 waveguide), which excites the lowest order quasi-transverse-electric (TE_{00}) mode of the waveguide. We record the spectrum at many increments of the input power using an automated system [33] that interfaces with both the rotation mount and the optical spectrum analyzers. The waveguide modes (and their effective indices) are calculated using a vector finite-difference mode-solver [34, 35], using published refractive indices for Si_3N_4 [36] and SiO_2 [37]. Further experimental details are found in the SM.

For the width-modulated waveguides, a narrow peak appears in the spectrum in the 630-nm region (Fig. 2a), and the location of this peak changes with the width-

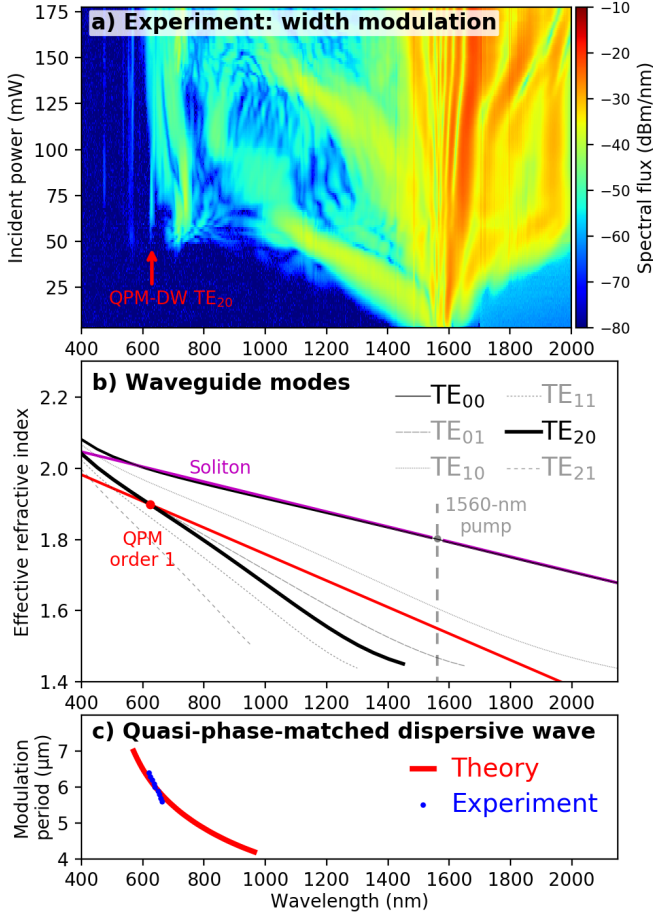


FIG. 2. a) The spectrum of supercontinuum generation from a width-modulated waveguide as a function of input power. The arrow indicates the quasi-phase-matched dispersive wave (QPM-DW) to the TE₂₀ mode. b) The effective refractive index of various modes of the waveguide as a function of wavelength. When the index of the soliton including a first order grating effect from the 6.2- μm width-modulation (red line) crosses the TE₂₀ mode, a QPM-DW is generated. c) The calculated spectral location of the TE₂₀ QPM-DW as a function of the width-modulation period is in agreement with experimental results. The slight difference in slope may arise from irregularities in the dimensions of the waveguides.

modulation period (Fig. 2c). By calculating the refractive index of the higher order modes of the waveguide, and including the QPM effect from the periodic width modulation (Fig. 2b and Eq. 2), we find the QPM-DW generation to the TE₂₀ mode is a likely mechanism for the appearance of this peak (Fig. 2c). The preference for QPM-DW generation to the TE₂₀ mode is a result of the modal overlap [3, 38] (Fig. 3) between the TE₂₀ mode at the DW wavelength (~ 630 nm) and the TE₀₀ mode at the soliton wavelength (1560 nm). In general, modes that are symmetric in both the vertical and horizontal (such as the TE₂₀ mode) will have much higher overlap to the fundamental mode than antisymmetric modes (see SM, section III), and are consequently the most commonly

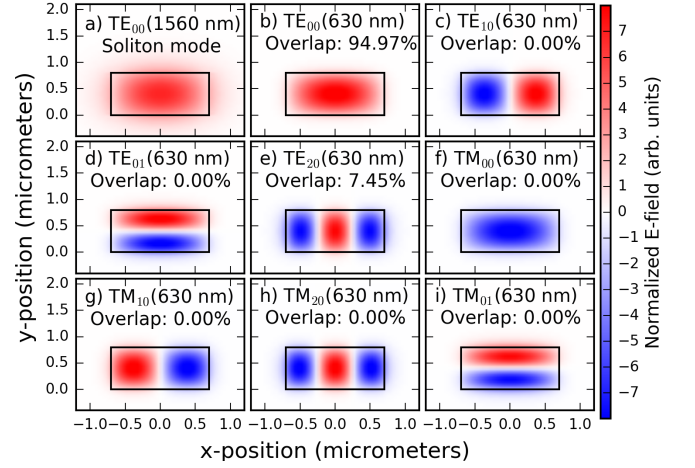


FIG. 3. Electric field profiles for the waveguide modes for a fully SiO₂-clad Si₃N₄ waveguide. a) The TE₀₀ mode at 1560 nm, which is the expected mode of the soliton. b-i) The electric field for various higher order modes at 630 nm, which is the approximate wavelength for the QPM-DW observed for the width-modulated waveguides. The result of the overlap integral of each mode with the TE₀₀ mode at 1560 nm is listed. Only the TE₀₀ and TE₂₀ modes have overlap integrals that are not vanishingly small. Note: for TM modes, E_y is shown, while E_x is shown for TE modes.

used for model phase-matching schemes [39].

For the cladding-modulated waveguides, many QPM-DW peaks are seen in the supercontinuum spectrum (Fig 4a). In some cases, the enhancement in the spectral intensity is as high as 20 dB. Similarly to the width-modulated waveguides, an analysis of the refractive index profile indicates that the TE₂₀ mode is responsible for the QPM-DW generation (Fig. 4). Interestingly, peaks are observed corresponding to both odd- and even-order QPM, and effects up to the 16th QPM order are detectable. This situation differs from the preference for low, odd-ordered QPM effects in typical QPM materials (such as periodically poled lithium niobate, PPLN [26]), which usually employ a 50-percent duty-cycle modulation. In contrast, the cladding-modulated Si₃N₄ waveguides have short regions of oxide cladding, followed by long regions of fully air-clad Si₃N₄. This high-duty-cycle square wave is composed of both even- and odd-order harmonics, and consequently provides both even- and odd-order QPM. The simulated QPM-DW positions are in good agreement with the experiment for all grating orders and waveguide widths. Importantly, we see that QPM can still produce strong DWs with QPM orders of 8 or more, indicating that QPM for strongly phase-mismatched processes could be achieved with higher-order QPM instead of short modulation periods, potentially avoiding fabrication difficulties and scattering loss. We also observe QPM-DW generation to the TE₀₀ mode (Fig. 4a), which is reproduced by numerical simulations using the nonlinear schrödinger equation [40–42] (See Supplementary Material, Fig. S2).

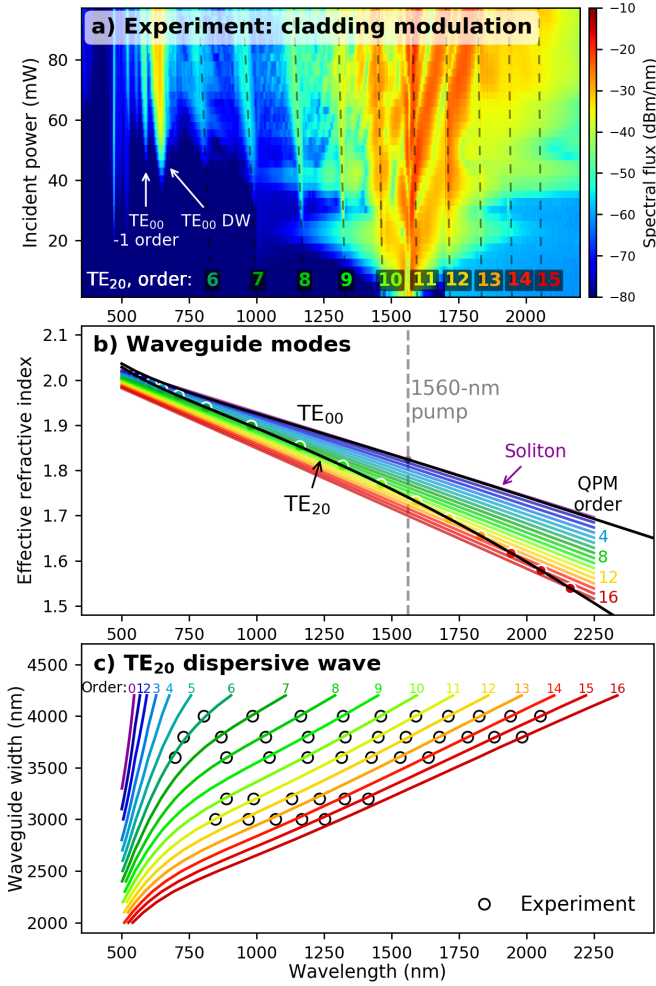


FIG. 4. a) Supercontinuum generation from a 4000-nm-width cladding-modulated waveguide, showing many QPM-DW peaks resulting from QPM orders 6-to-15 to the TE₂₀ mode. The locations of the QPM-DWs predicted by theory (dashed lines) agree with the experiment. DWs corresponding to phase-matching to the soliton and to -1 order QPM to the TE₀₀ mode are indicated with arrows. b) The effective index of the TE₀₀ and TE₂₀ modes, compared with the effective index of the soliton for various QPM orders (colorful lines). The dots indicate the location of the QPM-DW in the TE₂₀ mode. c) Calculations indicate that the locations of the QPM-DWs change as a function of waveguide width, in agreement with experiment. Note: the sharp peaks in the 530-nm region of (a) are a result of third-harmonic generation to higher-order spatial modes [17].

This is the first demonstration of QPM to produce DWs in on-chip waveguides, but it is interesting to note that the QPM-DWs have been observed in a variety of situations. Indeed, the “Kelly sidebands” [43] seen in laser cavities and sidebands seen during soliton propagation in long-distance fiber links [44] are both examples of QPM-DWs. QPM has also been demonstrated for both modulation-instability as well as soliton-DW phase-matching using width-oscillating fibers [27, 29, 31] and

for fiber-Bragg gratings [45–49]. QPM has also been seen in Kerr frequency comb generation [50]. On-chip waveguides provide a powerful new platform for QPM-DW generation, offering straightforward dispersion engineering, access to a range of modulation periods, scalable fabrication, and the ability to access well-defined higher-order modes.

In this first demonstration, the spectral brightness of the QPM-DWs was limited by several factors. First, most of the QPM-DWs were generated in the TE₂₀ mode, which doesn’t have optimal overlap with the TE₀₀ mode. Indeed, in the case where a -1-order QPM-DW is generated in the TE₀₀ mode (Fig. 4a), the intensity of the light is higher. Second, for the cladding-modulated waveguides, we rely on a QPM structure with a high duty cycle, which effectively spreads the available QPM efficiency over many QPM orders, sacrificing efficiency in one particular order. Third, our waveguides only made modest changes to the effective mode area, and stronger QPM could be likely achieved with a deeper width modulation or stronger change in the cladding index. Finally, the QPM-DWs are often produced far from the pump wavelength, in a spectral region where the soliton is dim. In future designs, optimized strategies for QPM-DW generation could utilize somewhat longer modulation periods, allowing QPM to the TE₀₀ mode, thereby maximizing mode-overlap and allowing the QPM-DWs to be located closer to the soliton central wavelength. Additionally, the waveguide modulation could be designed such that the efficiency of ± 1 order QPM is optimized. All of these parameters can be modeled using software that calculates the modes of the waveguide. This fact, combined with the massive scalability of lithographic processing, should allow for rapid progress in designing optimized photonic waveguides for SCG.

Currently, designers of waveguide-SCG sources work in a limited parameter space: selecting materials and selecting the dimensions of the waveguide cross section. QPM opens a new dimension in the design-space for photonic waveguides, one that is largely orthogonal to the other design dimensions. This orthogonality exists both in real-space, since the QPM-modulations exist in the light-propagation direction, but also in the waveguide-design-space, as it provides a simple vertical shift of the phase-matching conditions with no bending of the index curve (Fig. 1c). Consequently, it allows the spectral location of DWs to be modified with minimal effect on the GVD at the pump wavelength, which enables the soliton propagation conditions to be controlled separately from the DW phase-matching conditions. For example, using QPM, DWs could be produced even for purely anomalous GVD, greatly relaxing the requirements for material dispersion and waveguide cross section. Importantly, since the GVD at the pump is known to affect the noise properties of the SCG process [2], the ability to manipulate the locations of the DWs separately from the GVD could enable SCG sources that are simultaneously broadband and low-noise. In addition, since similar

phase-matching conditions apply to SCG with picosecond pulses or continuous-wave lasers [2], QPM of the SCG process is likely not restricted to the regime of femtosecond pulses.

In summary, here we demonstrated that quasi-phase-matching is a powerful tool for controlling the supercontinuum generation process in on-chip photonic waveguides. We experimentally verified that a periodic modulation of either the waveguide width or cladding can allow Si_3N_4 waveguides to produce dispersive wave light at tunable spectral locations. By allowing dispersive waves to be quasi-phase-matched without significantly modifying the dispersion at the pump wavelength, this approach provides independent control over soliton compression and the spectral location of dispersive waves. Thus, quasi-phase-matching provides a new dimension in the design-space for on-chip waveguides and allows supercontinuum sources to be tailored for the specific needs of each application.

ACKNOWLEDGMENTS

We thank Jordan Stone, Nate Newbury, Michael Lombardi, and Chris Oates for providing helpful feedback on this manuscript. We thank Alexandre Kudlinski for his insightful comments on a draft of this manuscript. This work is supported by AFOSR under award number FA9550-16-1-0016, DARPA (DODOS and ACES programs), NIST, and NRC. This work is a contribution of the U.S. government and is not subject to copyright in the U.S.A.

Supplemental Materials: Quasi-phase-matched supercontinuum-generation in photonic waveguides

I. WAVEGUIDE FABRICATION

The width-modulated Si_3N_4 waveguides were fabricated by Ligentec, using the “Photonic Damascene” process [51]. They are fully SiO_2 -clad, and have a thickness of 750 nm, and a maximum width of 1500 nm. The end-sections are tapered to 150 nm at the input and exit facets in order to expand the mode and allow for improved coupling efficiency, which is typically -2 dB per facet. The overall length of the waveguides is 15 mm, and, over a 6-mm central region, the width is modulated sinusoidally from 1250 to 1500 nm. The modulation period ranges from 5.5 to 6.5 μm .

The “suspended” cladding-modulated waveguides were fabricated at NIST Gaithersburg. First, 700 nm of Si_3N_4 was deposited onto thermally oxidized silicon wafers using low pressure chemical vapor deposition (LPCVD), and the waveguides were patterned with electron-beam lithography and reactive ion etching. Plasma enhanced chemical vapor deposition (PECVD) was then used to selectively deposit a SiO_2 cladding on the input and output coupling regions. The sample was then coated with photoresist and patterned to define the suspended regions. After development, the sample was soaked for 30 minutes in a 6:1 solution of buffered oxide etch (BOE) to release the waveguides. The waveguides are 12 mm in total length, and the first and last 0.5 mm are clad with SiO_2 in order to provide a symmetric mode profile that improves coupling efficiency. The SiO_2 supports are on a pitch of 200 μm and are in contact with the Si_3N_4 waveguide for approximately 20 μm .

II. EXPERIMENT

The light is coupled into each waveguide using an aspheric lens (numerical aperture of 0.6) designed for 1550 nm. The light is collected by butt-coupling an InF_3 multimode fiber (numerical aperture of 0.26) at the exit facet of the chip. The waveguide output is then recorded using two optical spectrum analyzers (OSAs); a grating-based OSA (Ando 6315E) is used for the spectrum across the visible and near-infrared regions, while a Fourier-transform OSA (Thorlabs OSA205) extends the coverage to 5600 nm. The angle of the half-waveplate is controlled using a Thorlabs K10CR1 rotation stage.

For easy visualization of the spectral enhancement due to QPM, Fig. S1 shows representative spectra from both the width-modulated and cladding-modulated waveguides. These spectra are single rows of Fig. 2a and 4a in the main text and in each case, the QPM-enabled spectral peaks can have heights of 20 dB or more relative to the supercontinuum.

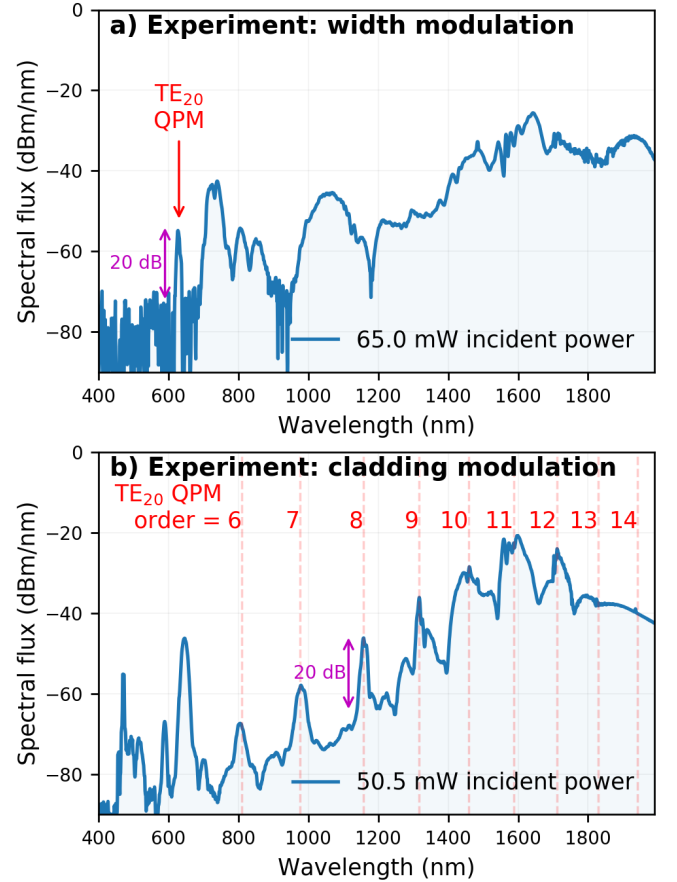


FIG. S1. Experimental supercontinuum spectra showing quasi-phase-matched dispersive-waves (QPM-DWs) due to waveguide modulation. a) Spectrum of the supercontinuum light produced from the width-modulated waveguide shown in Fig. 2a (6.2- μm width-modulation period) with 65.0 mW incident power. Enhancement of the spectral flux to the TE_{20} mode can be seen as a sharp peak near 630 nm. b) Spectrum of the supercontinuum light produced by the cladding-modulated waveguide shown in Fig. 4a (width of 4000-nm) with 50.5 mW of incident power. Numerous QPM orders can be seen with peak heights of >20 dB in some cases. The dashed red lines show the theoretically predicted position of each TE_{20} QPM order.

III. WAVEGUIDE MODES

We label the quasi-transverse-electric (TE, horizontal polarization) and quasi-transverse-magnetic (TM, vertical polarization) waveguides modes using subscripts that indicate the number of nodes in the x - and y -directions respectively (Fig. 3). For example, the TE_{20} mode (Fig. 3e) has two nodes in the x -direction and zero nodes in the y -direction. Experimentally, we observe quasi-phase-matched dispersive wave (QPM-DW) generation from the TE_{00} mode to the TE_{20} , which seems somewhat

counter-intuitive, since in a waveguide, all modes *at the same wavelength* are orthogonal. However, it is possible for one mode at a certain wavelength to have a nonzero overlap with other modes at a different wavelength. For a simple rectangular waveguide with symmetric cladding (Fig. 3), overlap to the TE_{00} mode can only occur for symmetric modes, i.e., modes that have even numbers of x and y nodes (where zero is an even number). For example, if we consider the antisymmetric TE_{10} mode (Fig. 3c), we find that the mode overlap integral will be strictly zero, since any overlap on the right side will be precisely canceled by the antisymmetric left side. In contrast, the TE_{20} mode (Fig. 3e) can have nonzero overlap with the TE_{00} mode. Thus, to generate light into higher order modes using a lowest-order-mode pump, symmetric modes such as the TE_{20} mode offer the best overlap [39].

IV. QPM MECHANISM

The width- and cladding-modulated waveguides provide QPM for the DW phase-matching condition. However, the experimental results do not specify if the effect is due to the modulation of the intensity of the light (and therefore modulation of the effective nonlinearity of the waveguide, γ) or if it is due to the modulation of the waveguide group-velocity dispersion (GVD), which changes the effective phase-mismatch for soliton-DW phase-matching along the waveguide length. Depending on the specific situation, it is conceivable that either effect causes the experimentally observed QPM.

Thus, we employ numerical solutions to the Nonlinear Schrödinger equation (NLSE) [40–42] to investigate which effect plays the most important role for our waveguides. We run NLSE simulations in three cases:

1. Including the modulation of both the GVD and γ ,
2. Including the modulation of γ only,
3. Including the modulation of the GVD only.

Our simulations only consider the fundamental mode of the waveguide and do not take into account effects due to higher order modes, which prevents them from modeling the QPM-DWs in the TE_{20} mode.

Fortunately, in the case of the cladding-modulated waveguides, QPM-DWs to the fundamental (TE_{00}) mode are experimentally observed on the short-wavelength side

of the main DW (Fig. 4a). These features are reproduced by the NLSE (Fig. S2a,c) *only* when the modulation of the GVD is taken into account. When the simulations include the modulation of γ alone, no obvious QPM effects are seen, suggesting that for the cladding-modulated waveguides, phase-matching is enabled by GVD modulation.

For the width modulated waveguides, the only experimentally observed QPM-DWs are those in the TE_{20} mode, and thus we do not attempt to precisely model the experiment, since the simulations do not take into account higher order modes. Instead, we model a waveguide with a similar sinusoidal width modulation (1250 to 1500 nm), but with a modulation period of 80 μm , which enables a QPM-DW in the TE_{00} mode. Again, the NLSE indicates that the modulation of the GVD is the dominant effect (Fig. S2b,d), in agreement with previous studies of QPM-DW generation [27, 29, 31]. We expect that the GVD will also provide QPM for the QPM-DWs in the TE_{20} mode.

This method of QPM via GVD modulation can be understood by considering that the soliton and the DW are phase-mismatched, and that the GVD determines the degree of mismatch. As a result, the DW light experiences regions of constructive and destructive interference along the length of the waveguide. By modulating the GVD, the regions of constructive interference can be made slightly longer than the regions of destructive interference. The net result is that, while the intensity of the DW still oscillates to some degree, there is a constructive build-up of light intensity [31]. The oscillation and build-up of the QPM-DW light as a function of propagation length can be seen in Figs. S2c and S2d in a region near the point of soliton fission (approximately 3 mm in Fig. S2b and 2 mm in Fig. S2d).

V. DISCLAIMER

Certain commercial equipment, instruments, or materials are identified here in order to specify the experimental procedure adequately. Such identification is not intended to imply recommendation or endorsement by the National Institute of Standards and Technology, nor is it intended to imply that the materials or equipment identified are necessarily the best available for the purpose. This work is a contribution of the United States government and is not subject to copyright in the United States of America.

[1] Robert R. Alfano, *The Supercontinuum Laser Source - The Ultimate White Light* | Robert R. Alfano | Springer, 3rd ed. (Springer, 2016).
 [2] John M. Dudley, Göry Genty, and Stéphane Coen, "Supercontinuum generation in photonic crystal fiber," *Reviews of Modern Physics* **78**, 1135–1184 (2006).

[3] Govind P. Agrawal, *Nonlinear Fiber Optics* (Academic Press, 2007).
 [4] David J. Jones, Scott A. Diddams, Jinendra K. Ranka, Andrew Stentz, Robert S. Windeler, John L. Hall, and Steven T. Cundiff, "Carrier-Envelope Phase Control of Femtosecond Mode-Locked Lasers and Direct Optical

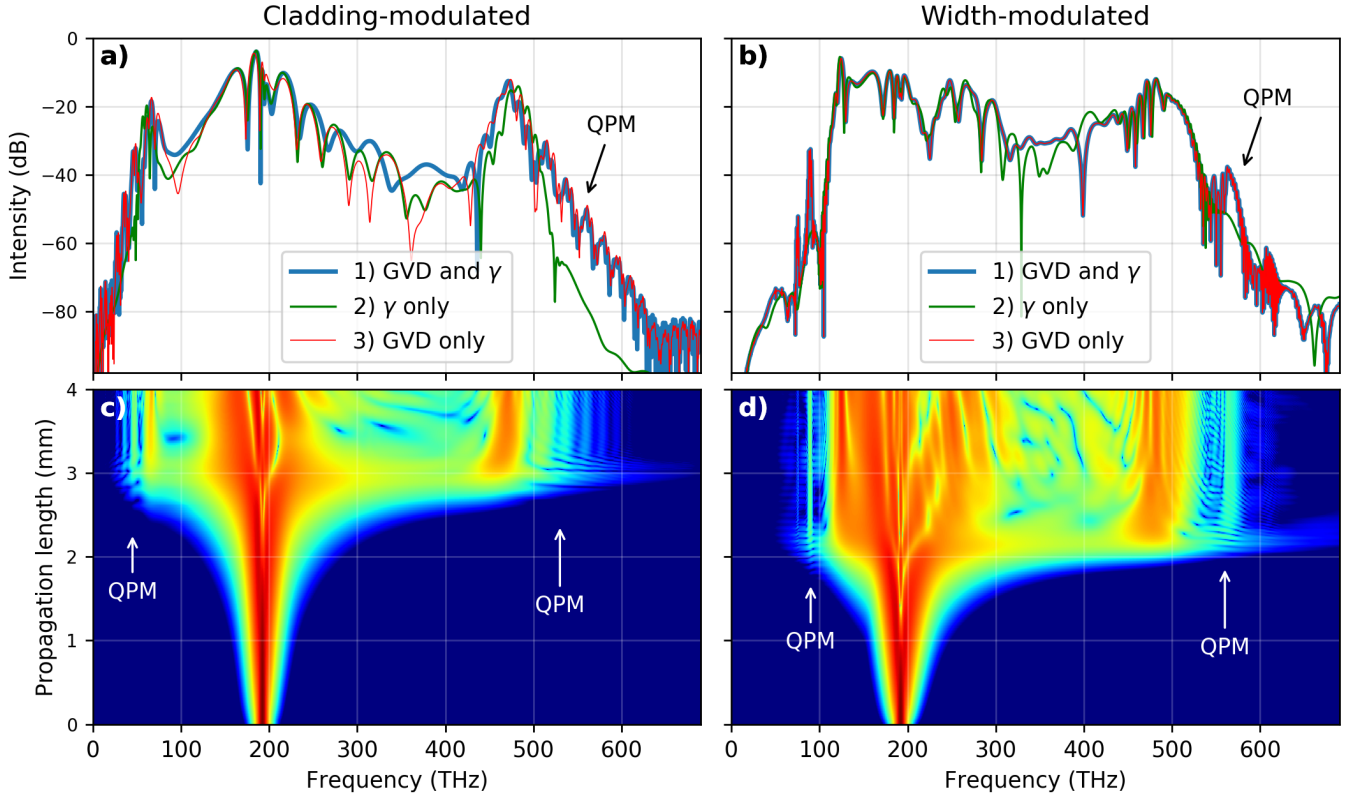


FIG. S2. Numerical simulations using the Nonlinear Schrödinger Equation (NLSE) for 80-fs, 300-pJ pulses propagating through cladding-modulated (left) and width-modulated (right) waveguides. a,b) QPM effects can be seen in the case where modulations to the group velocity dispersion (GVD) alone are included and in the situation where modulation of the GVD and the effective nonlinearity “GVD and γ ” are included. However, only including modulations to γ is not sufficient to achieve QPM. c,d) The spectrum as a function of propagation length along the waveguide. In the region of soliton fission, the intensity of the QPM-DWs oscillates as a function of propagation length. **Simulation parameters:** The cladding-modulated waveguides are modeled using values from the experiment: a thickness of 700 nm, a width of 4000 nm, with periodic SiO₂ bottom-cladding with a length of 20 μ m on a 200 μ m pitch. The width-modulated waveguides are modeled using height (650 nm) and width (sinusoidal variation between 1250 and 1500 nm) values from experiment, but with a modulation period of 80 μ m in order to show QPM-DW generation to the TE₀₀ mode.)

- Frequency Synthesis,” *Science* **288**, 635–639 (2000).
- [5] R. Holzwarth, Th. Udem, T. W. Hansch, J. C. Knight, W. J. Wadsworth, and P. St. J. Russell, “Optical Frequency Synthesizer for Precision Spectroscopy,” *Physical Review Letters* **85**, 2264–2267 (2000).
- [6] Scott A. Diddams, David J. Jones, Jun Ye, Steven T. Cundiff, John L. Hall, Jinendra K. Ranka, Robert S. Windeler, Ronald Holzwarth, Thomas Udem, and T. W. Hansch, “Direct Link between Microwave and Optical Frequencies with a 300 THz Femtosecond Laser Comb,” *Physical Review Letters* **84**, 5102–5105 (2000).
- [7] Timo Betz, Jorn Teipel, Daniel Koch, Wolfgang Hartig, Jochen R. Guck, Josef Käs, and Harald W. Giessen, “Excitation beyond the monochromatic laser limit: simultaneous 3-D confocal and multiphoton microscopy with a tapered fiber as white-light laser source,” *Journal of Biomedical Optics* **10**, 054009 (2005).
- [8] Ian Coddington, Nathan Newbury, and William Swann, “Dual-comb spectroscopy,” *Optica* **3**, 414–426 (2016).
- [9] Sucbei Moon and Dug Young Kim, “Ultra-high-speed optical coherence tomography with a stretched pulse supercontinuum source,” *Optics Express* **14**, 11575–11584 (2006).
- [10] Alexander Klenner, Aline S. Mayer, Adrea R. Johnson, Kevin Luke, Michael R. E. Lamont, Yoshitomo Okawachi, Michal Lipson, Alexander L. Gaeta, and Ursula Keller, “Gigahertz frequency comb offset stabilization based on supercontinuum generation in silicon nitride waveguides,” *Optics Express* **24**, 11043–11053 (2016).
- [11] Marco A. G. Porcel, Florian Schepers, Jörn P. Epping, Tim Hellwig, Marcel Hoekman, René G. Heideman, Peter J. M. van der Slot, Chris J. Lee, Robert Schmidt, Rudolf Bratschitsch, Carsten Fallnich, and Klaus-J. Boller, “Two-octave spanning supercontinuum generation in stoichiometric silicon nitride waveguides pumped at telecom wavelengths,” *Optics Express* **25**, 1542–1554 (2017).
- [12] A. S. Mayer, A. Klenner, A. R. Johnson, K. Luke, M. R. E. Lamont, Y. Okawachi, M. Lipson, A. L. Gaeta, and U. Keller, “Frequency comb offset detection using supercontinuum generation in silicon nitride waveguides,” *Optics Express* **23**, 15440–15451 (2015).

- [13] Jorn P. Epping, Tim Hellwig, Marcel Hoekman, Richard Mateman, Arne Leinse, René G. Heideman, Albert van Rees, Peter J. M. van der Slot, Chris J. Lee, Carsten Fallnich, and Klaus-J. Boller, “On chip visible-to-infrared supercontinuum generation with more than 495 THz spectral bandwidth,” *Optics Express* **23**, 19596–19604 (2015).
- [14] Bart Kuyken, Takuro Ideguchi, Simon Holzner, Ming Yan, Theodor W. Hänsch, Joris Van Campenhout, Peter Verheyen, Stéphane Coen, François Leo, Roel Baets, Gunther Roelkens, and Nathalie Picqué, “An octave-spanning mid-infrared frequency comb generated in a silicon nanophotonic wire waveguide,” *Nature Communications* **6** (2015), 10.1038/ncomms7310.
- [15] J. M. Chavez Boggio, D. Bodenmüller, T. Fremberg, R. Haynes, M. M. Roth, R. Eisermann, M. Lisker, L. Zimmermann, and M. Böhm, “Dispersion engineered silicon nitride waveguides by geometrical and refractive-index optimization,” *JOSA B* **31**, 2846–2857 (2014).
- [16] David Carlson, Daniel Hickstein, Alexander Lind, Judith Olson, Richard Fox, Roger Brown, Andrew Ludlow, Qing Li, Daron Westly, Holly Leopardi, Tara Fortier, Kartik Srinivasan, Scott Diddams, and Scott Papp, “Photonic-Chip Supercontinuum with Tailored Spectra for Counting Optical Frequencies,” *Physical Review Applied* **8**, 014027 (2017).
- [17] David R. Carlson, Daniel D. Hickstein, Alex Lind, Stefan Droste, Daron Westly, Nima Nader, Ian Coddington, Nathan R. Newbury, Kartik Srinivasan, Scott A. Diddams, and Scott B. Papp, “Self-referenced frequency combs using high-efficiency silicon-nitride waveguides,” *Optics Letters* **42**, 2314–2317 (2017).
- [18] Dong Yoon Oh, Ki Youl Yang, Connor Fredrick, Gabriel Ycas, Scott A. Diddams, and Kerry J. Vahala, “Coherent ultra-violet to near-infrared generation in silica ridge waveguides,” *Nature Communications* **8** (2017), 10.1038/ncomms13922.
- [19] Daniel D. Hickstein, Hojoong Jung, David R. Carlson, Alex Lind, Ian Coddington, Kartik Srinivasan, Gabriel G. Ycas, Daniel C. Cole, Abijith Kowligy, Connor Fredrick, Stefan Droste, Erin S. Lamb, Nathan R. Newbury, Hong X. Tang, Scott A. Diddams, and Scott B. Papp, “Ultrabroadband Supercontinuum Generation and Frequency-Comb Stabilization Using On-Chip Waveguides with Both Cubic and Quadratic Nonlinearities,” *Physical Review Applied* **8**, 014025 (2017).
- [20] R. Driben, A. V. Yulin, and A. Efimov, “Resonant radiation from oscillating higher order solitons,” *Optics Express* **23**, 19112–19117 (2015).
- [21] J. McLenaghan and F. König, “Few-cycle fiber pulse compression and evolution of negative resonant radiation,” *New Journal of Physics* **16**, 063017 (2014).
- [22] Nail Akhmediev and Magnus Karlsson, “Cherenkov radiation emitted by solitons in optical fibers,” *Physical Review A* **51**, 2602–2607 (1995).
- [23] Robert W. Boyd, *Nonlinear Optics, Third Edition*, 3rd ed. (Academic Press, Amsterdam ; Boston, 2008).
- [24] P. A. Franken and J. F. Ward, “Optical Harmonics and Nonlinear Phenomena,” *Reviews of Modern Physics* **35**, 23–39 (1963).
- [25] J. A. Armstrong, N. Bloembergen, J. Ducuing, and P. S. Pershan, “Interactions between Light Waves in a Nonlinear Dielectric,” *Physical Review* **127**, 1918–1939 (1962).
- [26] M. M. Fejer, G. A. Magel, D. H. Jundt, and R. L. Byer, “Quasi-phase-matched second harmonic generation: tuning and tolerances,” *IEEE Journal of Quantum Electronics* **28**, 2631–2654 (1992).
- [27] Alexandre Kudlinski, Arnaud Mussot, Matteo Conforti, and Stefano Trillo, “Parametric excitation of multiple resonant radiations from localized wavepackets,” *Scientific Reports* **5**, 9433 (2015).
- [28] Kathy Luo, Yiqing Xu, Miro Erkintalo, and Stuart G. Murdoch, “Resonant radiation in synchronously pumped passive Kerr cavities,” *Optics Letters* **40**, 427–430 (2015).
- [29] M. Conforti, S. Trillo, A. Kudlinski, and A. Mussot, “Multiple QPM Resonant Radiations Induced by MI in Dispersion Oscillating Fibers,” *IEEE Photonics Technology Letters* **28**, 740–743 (2016).
- [30] Logan G. Wright, Stefan Wabnitz, Demetrios N. Christodoulides, and Frank W. Wise, “Ultrabroadband Dispersive Radiation by Spatiotemporal Oscillation of Multimode Waves,” *Physical Review Letters* **115**, 223902 (2015).
- [31] M. Droques, A. Kudlinski, G. Bouwmans, G. Martinelli, and A. Mussot, “Dynamics of the modulation instability spectrum in optical fibers with oscillating dispersion,” *Physical Review A* **87**, 013813 (2013).
- [32] L. C. Sinclair, J.-D. Deschênes, L. Sonderhouse, W. C. Swann, I. H. Khader, E. Baumann, N. R. Newbury, and I. Coddington, “A compact optically coherent fiber frequency comb,” *Review of Scientific Instruments* **86**, 081301 (2015).
- [33] Daniel D. Hickstein, Grace Kerber, Connor Fredrick, and David R. Carlson, “GracefulOSA,” <https://github.com/DanHickstein/gracefulOSA> (2017).
- [34] A. B. Fallahkhair, K. S. Li, and T. E. Murphy, “Vector Finite Difference Modesolver for Anisotropic Dielectric Waveguides,” *Journal of Lightwave Technology* **26**, 1423–1431 (2008).
- [35] Lorenzo Bolla, “EMPy - Electromagnetic Python,” <https://github.com/lbolla/EMPy> (2017).
- [36] Kevin Luke, Yoshitomo Okawachi, Michael R. E. Lamont, Alexander L. Gaeta, and Michal Lipson, “Broadband mid-infrared frequency comb generation in a Si₃N₄ microresonator,” *Optics Letters* **40**, 4823–4826 (2015).
- [37] I. H. Malitson, “Interspecimen Comparison of the Refractive Index of Fused Silica,” *JOSA* **55**, 1205–1209 (1965).
- [38] Q. Lin, Oskar J. Painter, and Govind P. Agrawal, “Nonlinear optical phenomena in silicon waveguides: Modeling and applications,” *Optics Express* **15**, 16604–16644 (2007).
- [39] Xiang Guo, Chang-Ling Zou, and Hong X. Tang, “Second-harmonic generation in aluminum nitride microrings with 2500%/W conversion efficiency,” *Optica* **3**, 1126–1131 (2016).
- [40] A. M. Heidt, “Efficient Adaptive Step Size Method for the Simulation of Supercontinuum Generation in Optical Fibers,” *Journal of Lightwave Technology* **27**, 3984–3991 (2009).
- [41] J. Hult, “A Fourth-Order Runge-Kutta in the Interaction Picture Method for Simulating Supercontinuum Generation in Optical Fibers,” *Journal of Lightwave Technology* **25**, 3770–3775 (2007).
- [42] Gabriel Ycas, Daniel Maser, and Daniel D. Hickstein, “pyNLO - Nonlinear optics modeling for Python,” (2016).

- [43] S. M. J. Kelly, “Characteristic sideband instability of periodically amplified average soliton,” *Electronics Letters* **28**, 806–807 (1992).
- [44] F. Matera, A. Mecozzi, M. Romagnoli, and M. Settembre, “Sideband instability induced by periodic power variation in long-distance fiber links,” *Optics Letters* **18**, 1499–1501 (1993).
- [45] P. S. Westbrook, J. W. Nicholson, K. S. Feder, Y. Li, and T. Brown, “Supercontinuum generation in a fiber grating,” *Applied Physics Letters* **85**, 4600–4602 (2004).
- [46] K. Kim, S. A. Diddams, P. S. Westbrook, J. W. Nicholson, and K. S. Feder, “Improved stabilization of a 1.3 μm femtosecond optical frequency comb by use of a spectrally tailored continuum from a nonlinear fiber grating,” *Optics Letters* **31**, 277–279 (2006).
- [47] L. M. Zhao, C. Lu, H. Y. Tam, D. Y. Tang, L. Xia, and P. Shum, “Observation of spectral enhancement in a soliton fiber laser with fiber Bragg grating,” *Optics Express* **17**, 3508–3513 (2009).
- [48] Dong-Il Yeom, Jeremy A. Bolger, Graham D. Marshall, Dane R. Austin, Boris T. Kuhlmeier, Michael J. Withford, C. Martijn de Sterke, and Benjamin J. Eggleton, “Tunable spectral enhancement of fiber supercontinuum,” *Optics Letters* **32**, 1644–1646 (2007).
- [49] P. S. Westbrook and J. W. Nicholson, “Perturbative approach to continuum generation in a fiber Bragg grating,” *Optics Express* **14**, 7610–7616 (2006).
- [50] Shu-Wei Huang, Abhinav Kumar Vinod, Jinghui Yang, Mingbin Yu, Dim-Lee Kwong, and Chee Wei Wong, “Quasi-phase-matched multispectral Kerr frequency comb,” *Optics Letters* **42**, 2110–2113 (2017).
- [51] Martin H. P. Pfeiffer, Arne Kordts, Victor Brasch, Michael Zervas, Michael Geiselmann, John D. Jost, and Tobias J. Kippenberg, “Photonic Damascene process for integrated high-Q microresonator based nonlinear photonics,” *Optica* **3**, 20–25 (2016).